

OH Zeeman Magnetic Field Detections Toward Five Supernova Remnants Using the VLA

C. L. Brogan¹, D. A. Frail², W. M. Goss², and T. H. Troland¹

ABSTRACT

We have observed the OH (1720 MHz) line in five galactic SNRs with the VLA to measure their magnetic field strengths using the Zeeman effect. We detected all 12 of the bright ($S_\nu > 200$ mJy) OH (1720 MHz) masers previously detected by Frail et al. (1996) and Green et al. (1997) and measured significant magnetic fields (i.e. $> 3\sigma$) in ten of them. Assuming that the “thermal” Zeeman equation can be used to estimate $|\vec{B}|$ for OH masers, our estimated fields range from 0.2 to 2 mG. These magnetic field strengths are consistent with the hypothesis that ambient molecular cloud magnetic fields are compressed via the SNR shock to the observed values. Magnetic fields of this magnitude exert a considerable influence on the properties of the cloud with the magnetic pressures ($10^{-7} - 10^{-9}$ erg cm⁻³) exceeding the pressure in the ISM or even the thermal pressure of the hot gas interior to the remnant. This study brings the number of galactic SNRs with OH (1720 MHz) Zeeman detections to ten.

Subject headings:

ISM:clouds — ISM:individual (W51, G349.7+0.2, CTB37A, CTB33, G357.7–0.1) — ISM:magnetic fields — masers — polarization — radio lines:ISM

¹University of Kentucky, Department of Physics & Astronomy, Lexington, KY 40506-0055

²National Radio Astronomy Observatory, P. O. Box O, 1003 Lopezville Road, Socorro, NM 87801

1. INTRODUCTION

Magnetic fields can moderate the impact that a shock has on a molecular cloud. In the absence of a field, a supernova blast wave will heat, compress and fragment the cloud and may ultimately destroy it (Klein, McKee & Colella 1994). The inclusion of a field mitigates these effects, limiting compression and stabilizing it against fragmentation, allowing the cloud to survive, perhaps to trigger a future generation of star formation (Miesch & Zweibel 1994; MacLow et al. 1994).

It has long been known that supernova remnants (SNRs) possess magnetic fields. Observations of synchrotron radiation have established that the *direction* of the magnetic field in young SNRs like Cas A is predominately parallel to the shock normal (i.e. radial), whereas for older remnants the fields are perpendicular (e.g. Dickel et al. 1991; Milne 1990). The latter geometry likely originates from the compression of the ambient interstellar field, while Rayleigh-Taylor instabilities are invoked to explain the radial fields in young SNRs (Jun & Norman 1996). Until recently, estimates of the *strength* of the magnetic fields in SNRs had to rely on the somewhat dubious equipartition approximation. This situation has changed with the re-discovery of shock-excited OH (1720 MHz) maser emission in SNRs (Frail, Goss & Slysh 1994).

In a series of recent papers, the satellite line of the OH molecule at 1720.53 MHz has been used as a powerful probe of SNR-molecular cloud interactions. OH (1720 MHz) masers are found in ~ 20 SNRs, or 10% of the known SNRs in our Galaxy (see Koralesky et al. 1998 and references therein). This maser line is inverted through collisions with H_2 ($n \sim \text{few} \times 10^4 \text{ cm}^{-3}$ and $T \sim 80 \text{ K}$) behind C-type shocks propagating into molecular clouds (Reach & Rho 1999, Frail & Mitchell 1998). The geometry of the shock is well constrained since strong maser amplification can only occur when the shock front is viewed edge on (Claussen et al. 1997). These observational statements are well-supported by theoretical modeling of the OH (1720 MHz) excitation (Lockett, Gauthier & Elitzur 1998; Wardle,

Yusef-Zadeh, & Geballe 1999; Wardle 1999).

One advantage of observing the OH (1720 MHz) maser line is that it allows for a measurement of the strength of the magnetic field via Zeeman splitting (e.g. Troland & Heiles 1982). In this case, when the observed splitting is small compared to the line width, $V = ZC|\vec{B}|dI/d\nu$, where $|\vec{B}|$ is the total magnetic field strength, Z is the Zeeman splitting coefficient, and C is a constant which depends on the angle between the line of sight and \vec{B} (the possible forms of C will be discussed in §4.1). For now we will denote the combination of $C|\vec{B}|$ as B_θ .

This method has already been used to successfully measure the magnetic field strength in the post-shock gas behind five SNRs (Sgr A East, W44, W28, G32.8–0.1, and G346.6–0.2), yielding values for B_θ between 0.1 to 4 mG (Yusef-Zadeh et al. 1996, Claussen et al. 1997, Koralesky et al. 1998). With these promising results in mind, we have performed 1720 MHz Zeeman studies toward five more of the 17 SNRs found in surveys by Frail et al. (1996) and Green et al. (1997) to contain OH (1720 MHz) masers using the NRAO³ VLA. Only SNRs with bright masers ($I > 200 \text{ mJy}$) and no previous high resolution Stokes V observations were chosen.

2. OBSERVATIONS

We observed five SNRs (W51, G349.7+0.2, CTB37A, CTB33, and G357.7–0.1) at 1720 MHz with the VLA in A configuration. The key observing parameters for each SNR are given in Table 1. All of the SNRs were observed in “2IF mode” (recording both right (RCP) and left (LCP) circular polarization) with a 0.1953 MHz (34.0 km s^{-1}) bandwidth divided into 127 channels. Due to this narrow bandwidth, CTB37A had to be observed with two different center frequencies (-22 km s^{-1} and -64 km s^{-1}) in order to obtain data for its two different OH (1720 MHz) maser populations. The observations were con-

³The National Radio Astronomy Observatory is a facility of the National Science Foundation operated under a cooperative agreement by Associated Universities, Inc.

TABLE 1
Observational Parameters with the VLA

SNR	R. A. ^a (B1950)	Decl. ^a (B1950)	V_{lsr} (km s ⁻¹)	t_{source} (hours)	Beam (" x ")	P. A. (°)	σ_{rms} ^b (mJy)
W51C (2IF)	19 20 35.0	+14 09 00.0	+64.0	3.3	1.4 x 1.2	-40	6.6
(PA) ^c	19 20 35.0	+14 09 00.0	+70.0	1.6	1.6 x 1.3	+55	6.5
G349.7+0.2	17 14 36.0	-37 22 00.0	+16.0	2.6	3.4 x 1.3	+08	7.2
CTB37A (I)	17 11 00.0	-38 30 00.0	-64.0	4.9	3.9 x 1.2	-14	5.4
(II)	17 11 00.0	-38 30 00.0	-22.0	4.0	4.2 x 2.3	+23	5.5
CTB33	16 32 14.0	-47 31 00.0	-70.0	2.1	8.0 x 1.1	+67	10.2
G357.7-0.1	17 36 56.0	-30 56 00.0	-12.0	5.1	3.0 x 1.2	+18	5.2

^aUnits of right ascension are hours, minutes, and seconds, and units of declination are degrees, arcminutes, and arcseconds.

^brms noise in an individual channel.

^cW51C (PA) data have a velocity resolution of 0.56 km s⁻¹ while all other data have velocity resolution of 0.27 km s⁻¹.

ducted on June 22, July 6, 8, 12, 15, September 13, and October 24, 1999. The OH data were Hanning smoothed online, and the resulting velocity resolution is 0.27 km s⁻¹. We observed both senses of circular polarization simultaneously and since Zeeman observations are very sensitive to small variations in the bandpass, a front-end transfer switch was used to periodically switch the sense of circular polarization passing through each telescope's IF system.

The AIPS (Astronomical Image Processing System) package of the NRAO was used for the calibration, imaging, and cleaning of the OH (1720 MHz) data sets. The RCP and LCP data were calibrated separately and later combined during the imaging process to make Stokes I=(RCP + LCP)/2 and Stokes V=(RCP - LCP)/2 data sets. Bandpass correction was applied only to the I data sets since bandpass effects cancel to first order in the V data. Line data sets were created by estimating and removing the continuum emission in the UV plane using the AIPS task UVLSF. The strongest maser channel in each line data set was then self-calibrated and the solutions were applied to each channel. Sub-

sequent magnetic field estimates were performed using the MIRIAD (Multichannel Image Reconstruction Image Analysis and Display) processing package from BIMA. The rms noise per spectral channel obtained for each SNR is summarized in Table 1.

After imaging, each of the bright maser spots was fit with a 2-D Gaussian using the AIPS task JMFIT. None of these fits showed convincing evidence that the individual maser spots are resolved at the resolutions shown in Table 1; therefore, we regard the maximum sizes reported by JMFIT to be upper limits. The positions, peak flux densities, and an upper limit to the maser spot sizes are reported in Table 2. In addition, the Stokes I spectrum at the peak pixel of each maser spot was fit with a single Gaussian in the spectral domain using GIPSY, to obtain each maser's center velocity (v) and linewidth (Δv_{FWHM}). These estimates of Δv_{FWHM} were then corrected for the finite channel width of the the data (0.27 km s⁻¹). These deconvolved Δv_{FWHM} and center velocities are also reported in Table 2. The absolute position errors of these data are $\sim 0.1''$, while the relative position er-

TABLE 2
Fitted Parameters of OH (1720 MHz) Masers

SNR	Feature	R. A. ^a (B1950)	Decl. ^a (B1950)	S_{peak} ^b (mJy)	v_{lsr} ^c (km s ⁻¹)	Δv_{FWHM} ^d (km s ⁻¹)	θ_{max} (")
W51C	1	19 20 35.9	+14 09 53.6	2710	+72.0	0.9	0.7
	2	19 20 36.4	+14 09 50.3	4760	+69.1	1.2	0.1
G349.7+0.2 ..	1	17 14 36.0	-37 23 01.9	770	+16.2	1.1	1.6
	2	17 14 36.9	-37 22 52.8	1800	+15.2	0.3	1.0
	3	17 14 37.5	-37 23 14.7	1060	+16.7	0.6	0.9
CTB37A	1	17 10 51.8	-38 28 51.7	410	-66.2	0.7	0.6
	2	17 10 56.8	-38 28 56.7	730	-63.7	0.5	0.3
	3	17 10 59.3	-38 31 19.2	470	-63.5	1.5	0.2
	4	17 11 01.4	-38 37 32.9	220	-65.3	1.1	0.7
	5	17 11 09.0	-38 25 51.3	400	-21.5	0.9	1.7
CTB33	1	16 32 06.2	-47 29 53.2	250	-71.8	1.0	1.7
G357.7-0.1 ..	1	17 36 54.6	-30 56 07.6	400	-12.3	0.6	0.8

^aUnits of right ascension are hours, minutes, and seconds, and units of declination are degrees, arcminutes, and arcseconds.

^bErrors in the peak flux range from 4 to 8 mJy.

^cErrors in v_{lsr} range from 0.02 to 0.002 km s⁻¹.

^dErrors in Δv_{FWHM} range from 0.05 to 0.003 km s⁻¹, and the values shown have been deconvolved from the finite channel width (0.27 km s⁻¹).

rors (compared to other masers in the field) are $\sim 0.02''$.

In addition, W51 was observed on August 3, 1999 in “PA mode” (recording all Stokes parameters) with a 0.1953 MHz bandwidth, and 64 channels. This correlator setup resulted in a velocity resolution of $\sim 0.54 \text{ km s}^{-1}$ after Hanning smoothing. The details of this observation can also be found in Table 1. These data were calibrated in the same manner described above, with the exception of the polarization calibration. The absolute polarization calibration was carried out by extrapolating 3C48 data from seven previous 20 cm polarimetry observations to yield a position angle of P.A. = 13° for this calibrator at 1720 MHz. The error in this estimate ($\sim 5^\circ$) will also apply to the position angles derived from these data.

3. RESULTS

3.1. General Maser Properties

From the five observed SNRs, we detected all 12 bright OH (1720 MHz) masers ($S > 200 \text{ mJy}$) previously known from the surveys of Frail et al. (1996) and Green et al. (1997). Table 2 summarizes the fitted parameters of these maser features. Of these, ten show classical S-shaped Stokes V profiles (e.g. Elitzur 1998), one shows a complicated Stokes V profile, and one shows no discernible V signal despite its $\sim 1800 \text{ mJy}$ peak flux density. The observed masers have typical deconvolved line widths of $\sim 0.8 \text{ km s}^{-1}$, spanning the range from 0.3 to 1.5 km s^{-1} . In addition, none of the observed OH (1720 MHz) masers appear to have undergone significant changes in flux density or position since the detection experiments were performed in 1994. As noted in §2, none of the maser spots have been resolved at the resolutions listed in Table 1. This may be due, in part, to the low declination, and hence elliptical synthesized beam shapes observed for four of the five SNRs. Using the upper limits on the maser spot sizes listed in Table 2, lower limits on the brightness temperatures of these masers range from $4 \times 10^4 \text{ K}$ to 10^8 K .

Using the thermal Zeeman expression ($V = ZC|\vec{B}|dI/d\nu$) with $Z = 0.6536 \text{ Hz } \mu\text{G}^{-1}$ for OH at 1720 MHz, the derivative of Stokes I was fitted to Stokes V in a least square fitting routine as described by Claussen et al (1997), to obtain the combination $C|\vec{B}| = B_\theta$. The validity of the thermal Zeeman formulation for the magnetic field in masers along with the θ dependence and magnitude of C is discussed in §4.1. Magnetic fields were detected toward all five SNR at greater than the 3σ level. The fitted magnetic field strengths (B_θ), and their associated 1σ errors are summarized in Table 3, while comments on individual sources appear in §3.2. The detected B_θ fields range from 0.2 to 2 mG. Unlike W28 and W44, where the fields were found to be uniform in both magnitude and direction (Claussen et al. 1997), CTB37A shows a complicated magnetic field morphology. In this source B_θ changes by a factor of seven and reverses sign on a length scale of $\sim 3 \text{ pc}$.

3.2. Individual Sources

3.2.1. W51

W51 is composed of two H II region complexes (W51A and W51B), as well as the SNR W51C and is located at the tangent point of the Sagittarius arm at $\ell = 49^\circ$ corresponding to a distance of $\sim 6 \text{ kpc}$ (Koo, Kim, & Seward 1995). A continuum image of W51 at 330 MHz from Subrahmanyan & Goss (1995) is shown in Figure 1 with the two W51 OH (1720 MHz) masers superposed. The spectral index of W51C is difficult to calculate due to contamination from the W51B H II regions, but Subrahmanyan & Goss (1995) estimate that $\alpha = -0.2$ ($S = \nu^\alpha$).

Based on the absorption of X-ray emission from W51C toward W51B, Koo et al. (1995) suggest that W51C must be located behind W51B. Koo & Moon (1997a, 1997b) observed high velocity (HV) H I, CO(1–0), and CO(2–1) emission between +85 and +120 km s^{-1} to the east of W51B where it overlaps W51C (see Fig. 1). They interpret this HV gas as arising from a shock interaction between W51C and a molecular cloud (located between W51C and W51B, or pos-

TABLE 3
Magnetic Fields

SNR	Feature	B_θ ^a (mG)
W51C	1	$+1.5 \pm 0.05$
	2	$+1.9 \pm 0.10$
G349.7+0.2 ...	1	complex ^b
	2	$\lesssim 0.1$ ^c
	3	-0.35 ± 0.05
CTB37A	1	-0.5 ± 0.10
	2	$+0.22 \pm 0.05$
	3	-0.60 ± 0.09
	4	$+1.5 \pm 0.20$
	5	-0.8 ± 0.10
CTB33	1	$+1.1 \pm 0.30$
G357.7-0.1 ...	1	$+0.7 \pm 0.12$

^aThese B_θ field estimates were calculated using the thermal Zeeman equation and may *overestimate* the maser fields according to the maser theory of Elitzur (1998). The correction cannot be determined exactly but is probably on the order of $(0.5 - 0.2) \times B_\theta$, therefore these values should be viewed as upper limits. See §4.1 for further discussion.

^bStokes V profile is complex, probably indicative of blending.

^cUpper limit to B_θ based on S/N of data. See also §3.2.2.

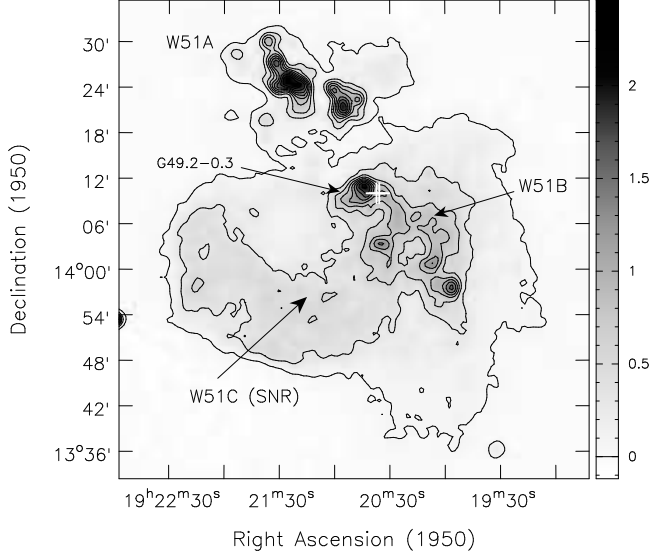


Fig. 1.— W51 VLA 330 MHz continuum image from Subrahmanyan & Goss (1995) with contours at $(0.02, 0.12, 0.22, 0.32, 0.42, 0.52, 0.62, 0.72, 0.82) \times 2.46 \text{ Jy beam}^{-1}$. The resolution of this image is $\sim 1'$. The locations of the two W51C OH (1720 MHz) masers are indicated by the white (+) symbols.

sibly the backside of the W51B complex itself). They show that the HV HI is located toward the western edge of the centrally bright X-ray emitting region of W51C in an arc-shape, while the shocked CO gas is located slightly east of the HV HI emission. The two OH (1720 MHz) masers reported in this work (and Green et al. 1997) are located toward the NE end of the shocked CO/HI arc structure and $\sim 2'$ SW of the HII region G49.2-0.3 (see Fig. 1) at velocities of $\sim 70 \text{ km s}^{-1}$. From the coincidence of these OH (1720 MHz) masers with the shocked gas and their angular separation from G49.2-0.3 ($\sim 3.5 \text{ pc}$ for $d = 6 \text{ kpc}$), Green et al. (1997) argue that they are associated with the W51C SNR shock.

Fits of B_θ for the two W51C OH (1720 MHz) masers are shown in Figure 2. The values of B_θ for these masers are 1.5 and 1.9 mG for features 1 and 2, respectively (see Tables 2 and 3). The W51C masers were also observed in PA mode, providing images of all four Stokes parameters (I, V, Q, U), with 0.54 km s^{-1} velocity resolution. Toward the strongest W51C OH maser (feature 2), Stokes Q and U signals were detected at 15σ

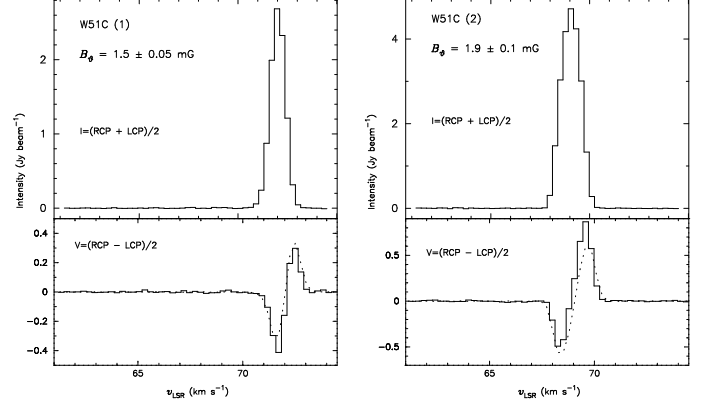


Fig. 2.— Fits of B_θ for W51 OH (1720 MHz) maser features (1) and (2). The upper panels show the VLA Stokes I profiles (*solid histogram*), and the bottom panels show the VLA Stokes V profiles (*solid histogram*) with the fitted derivative of Stokes I shown as smooth dotted curves. The value of B_θ fit for each position and its calculated error are given at the top of each plot.

and 17σ , respectively. A profile showing Stokes Q and U toward this maser is shown in Figure 3. Using Stokes Q and U values of $Q = 0.10 \text{ Jy beam}^{-1}$ and $U = -0.11 \text{ Jy beam}^{-1}$, we obtain a linear polarization percentage of 3.5% and a P.A. of -25° for the linear polarization vector.

3.2.2. G349.7+0.2

G349.7+0.2 is one of the most luminous SNR's in the galaxy (after Cas A and the Crab; Shaver et al. 1985a), if it is located at a distance of $\sim 22 \text{ kpc}$ (Frail et al. 1996). The spectral index of G349.7+0.2 was estimated by Shaver et al. (1985a) to be ~ -0.5 , typical of shell type remnants. This SNR contains three bright maser features along with several weaker features within $\sim 1'$ (6 pc) near the center of the remnant. The positions of the brightest masers are shown on a continuum image of G349.7+0.2 in Figure 4. This continuum image is a compilation of 18 and 20 cm data from the VLA archive, and contains data from all four configurations (A, B, C, and D). It is the most sensitive and highest resolution continuum image of this SNR to date, with a resolution of $5'' \times 2''$ (P.A. = 0.6°) and rms noise of $\sim 1 \text{ mJy beam}^{-1}$.

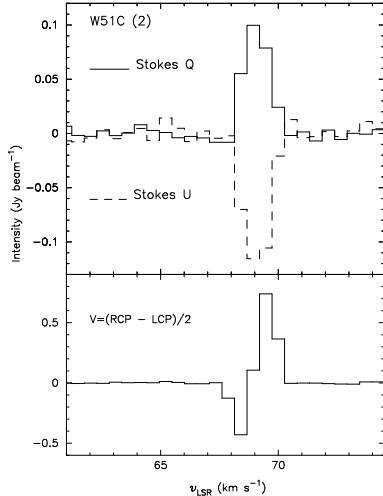


Fig. 3.— VLA Stokes Q and U linear polarization profiles (*upper panel*) and Stokes V circular polarization profile (*lower panel*) for W51C OH (1720 MHz) maser feature (2). Note that the spectral resolution of these data are only 0.56 km s^{-1} while the spectra displayed in Fig. 2 (and all other Figures) have a resolution of 0.27 km s^{-1} .

Only G349.7+0.2 OH(3) (OH maser feature 3) has a significant magnetic field detection with $B_\theta = 0.35 \text{ mG}$. The B_θ fit for this feature is shown in Figure 5. Maser features 1 and 2 are the only bright ($S > 200 \text{ mJy}$) OH (1720 MHz) masers in our sample for which we were unable to detect a significant B_θ . G349.7+0.2 OH(1) exhibits a complicated Stokes V spectrum that is indicative of blending. Therefore, it is possible that improved velocity and/or angular resolution would lead to a B_θ detection for this maser. G349.7+0.2 OH(2) shows no hint of any Stokes V signal despite its 1800 mJy flux density. The S/N of these data alone suggest that $B_\theta < 0.1 \text{ mG}$, however, this maser is also the narrowest maser in our sample ($\Delta v_{FWHM} = 0.3 \text{ km s}^{-1}$). Therefore, it is possible that if the Stokes V was not resolved in velocity, B_θ for G349.7+0.2 OH(2) could be $\sim 0.3 \text{ mG}$.

3.2.3. CTB37A

CTB37A, also known as G348.5+0.1, is estimated to lie at a distance of $\sim 11 \text{ kpc}$ (Frail et al. 1996). Kassim, Baum, & Weiler (1991) estimate its spectral index to be ~ -0.5 based on flux

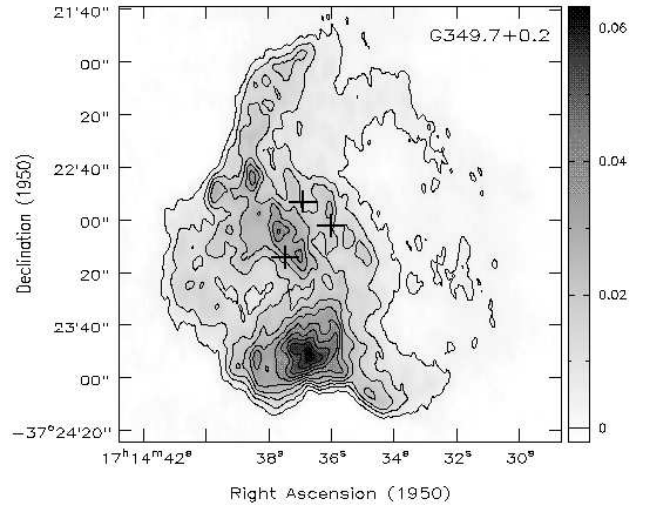


Fig. 4.— G349.7+0.2 20 cm VLA continuum image with contours at $(0.05, 0.15, 0.25, 0.35, 0.45, 0.55, 0.65, 0.75, 0.85, 0.95) \times 63 \text{ mJy beam}^{-1}$. This image is composed of archival VLA data from A, B, C, and D configurations. The resolution is $5'' \times 2''$ (P.A. = 0.6°) and the peak flux density is 63 mJy beam^{-1} with an rms noise of $\sim 1 \text{ mJy beam}^{-1}$. The locations of the three G349.7+0.2 OH (1720 MHz) masers with $S_\nu > 200 \text{ mJy}$ are indicated by the black (+) symbols.

density measurements ranging from 80 MHz to 14.7 GHz. A 21 cm continuum map of CTB37A from Kassim et al. (1991) is displayed in Figure 6 with the OH (1720 MHz) masers superposed. CTB37A contains two kinematically distinct sets of OH (1720 MHz) masers. One group at $\sim -22 \text{ km s}^{-1}$ is located toward the north end of CTB37A, while the others have velocities of $\sim -65 \text{ km s}^{-1}$ and are located near the center and southern parts of the source. Kassim et al. (1991) propose that the extension of continuum emission seen to the east of CTB37A (see Fig. 6) is a separate SNR which they name G348.5-0.0. It was further proposed by Frail et al. (1996) that the $\sim -22 \text{ km s}^{-1}$ masers originate from this second SNR.

CTB37A, also known as G348.5+0.1, is estimated to lie at a distance of $\sim 11 \text{ kpc}$ (Frail et al. 1996). Kassim, Baum, & Weiler (1991) estimate its spectral index to be ~ -0.5 based on flux density measurements ranging from 80 MHz to 14.7 GHz. A 21 cm continuum map of CTB37A

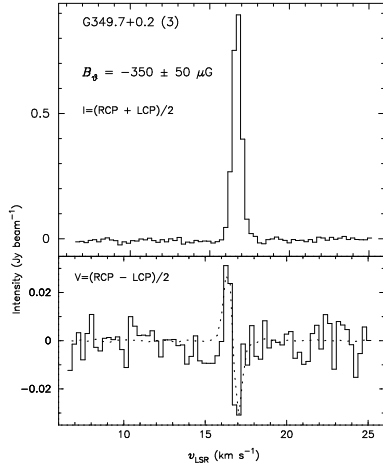


Fig. 5.— Fit of B_θ for G349.7+0.2 OH (1720 MHz) maser feature (3). The upper panels show the VLA Stokes I profiles (*solid histogram*), and the bottom panels show the VLA Stokes V profiles (*solid histogram*) with the fitted derivative of Stokes I shown as smooth dotted curves. The value of B_θ fit for each position and its calculated error are given at the top of each plot.

from Kassim et al. (1991) is displayed in Figure 6 with the OH (1720 MHz) masers superposed. CTB37A contains two kinematically distinct sets of OH (1720 MHz) masers. One group at ~ -22 km s $^{-1}$ is located toward the north end of CTB37A, while the others have velocities of ~ -65 km s $^{-1}$ and are located near the center and southern parts of the source. Kassim et al. (1991) propose that the extension of continuum emission seen to the east of CTB37A (see Fig. 6) is a separate SNR which they name G348.5-0.0. It was further proposed by Frail et al. (1996) that the ~ -22 km s $^{-1}$ masers originate from this second SNR.

As noted at the beginning of this section, the B_θ of the ~ -65 km s $^{-1}$ OH (1720 MHz) masers have the unusual property that they change direction along the line of site over length scales as small as $1'$ (~ 3 pc). In addition, the magnitude of B_θ changes by a factor of seven between CTB37A OH(2) and CTB37A OH(4) from ~ 0.2 mG to ~ 1.5 mG. Fits of B_θ for these four ~ -65 km s $^{-1}$ masers are shown in Figure 7. The only strong ~ -22 km s $^{-1}$ OH maser has $B_\theta = -0.8$ mG and the fit for this maser feature (CTB37A

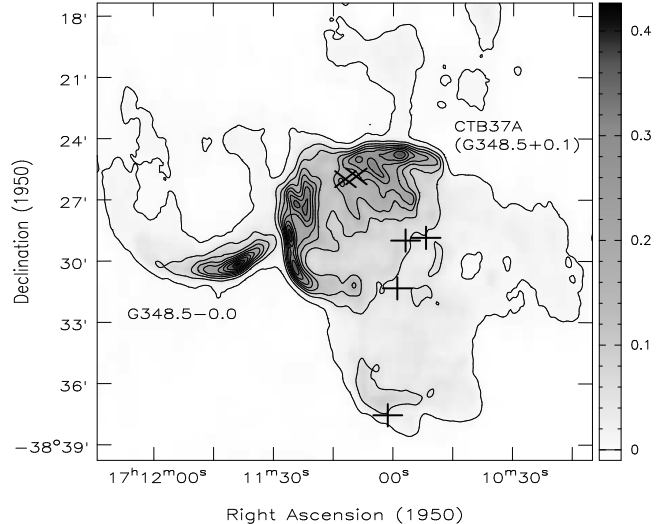


Fig. 6.— CTB37A 20 cm VLA continuum image from Kassim et al. (1991) with contours at (0.01, 0.12, 0.23, 0.34, 0.45, 0.56, 0.66, 0.76, 0.87) $\times 0.427$ Jy beam $^{-1}$. The beam is $33'' \times 18''$ (P.A. = 5°). The (+) symbols mark the locations of the ~ -65 km s $^{-1}$ OH (1720 MHz) maser features, while the locations of the ~ -22 km s $^{-1}$ OH (1720 MHz) maser features are marked with (x) symbols.

OH(5)) is also shown in Fig. 7.

Reynoso & Mangum (1999, in prep.) have detected CO(1-0) emission toward CTB37A with $\sim 1'$ resolution using the Kitt Peak 12m telescope. Their maps show two distinct CO clouds, one at ~ -22 km s $^{-1}$ in the northern part of CTB37A, and another at ~ -65 km s $^{-1}$ which is concentrated to the northwest and middle of the source. Both CO clouds are coincident spatially and in velocity with our two groups of OH (1720 MHz) masers.

As noted at the beginning of this section, the B_θ of the ~ -65 km s $^{-1}$ OH (1720 MHz) masers have the unusual property that they change direction along the line of site over length scales as small as $1'$ (~ 3 pc). In addition, the magnitude of B_θ changes by a factor of seven between CTB37A OH(2) and CTB37A OH(4) from ~ 0.2 mG to ~ 1.5 mG. Fits of B_θ for these four ~ -65 km s $^{-1}$ masers are shown in Figure 7. The only strong ~ -22 km s $^{-1}$ OH maser has $B_\theta = -0.8$ mG and the fit for this maser feature (CTB37A OH(5)) is also shown in Fig. 7.

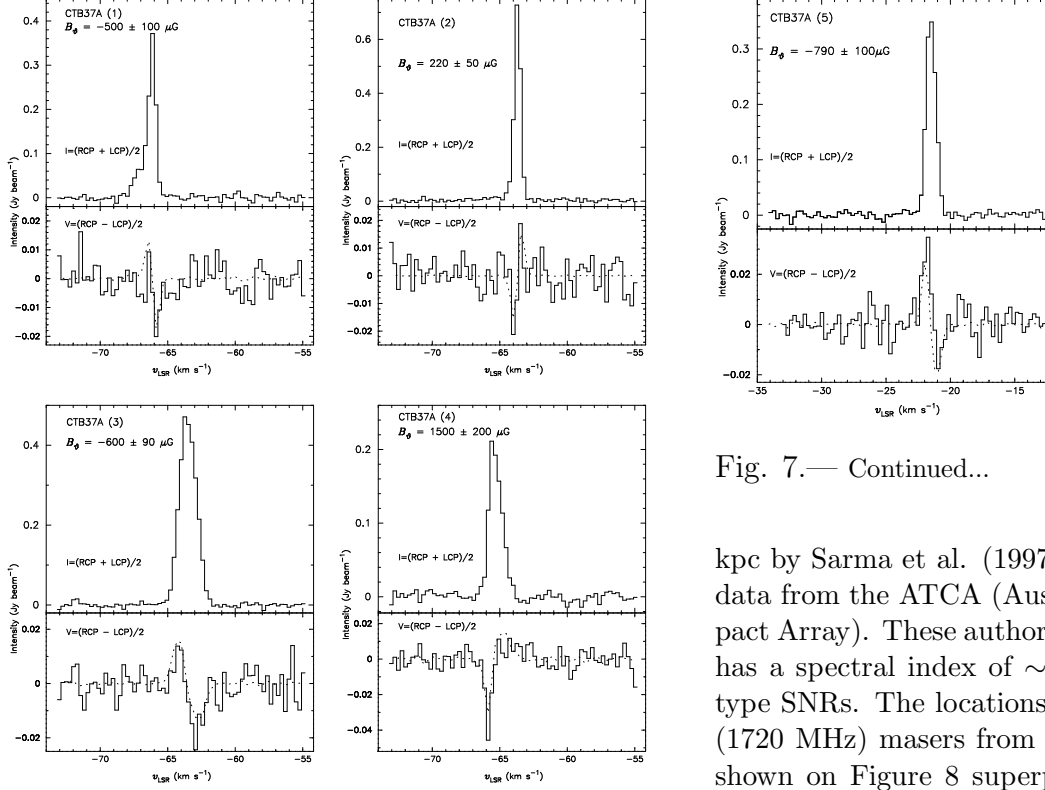


Fig. 7.— Fits of B_θ for CTB37A OH (1720 MHz) maser features (1 - 5). Note that features (1-4) correspond to the ~ -65 km s $^{-1}$ masers, while feature (5) is the single strong ~ -22 km s $^{-1}$ maser. The upper panels show the VLA Stokes I profiles (*solid histogram*), and the bottom panels show the VLA Stokes V profiles (*solid histogram*) with the fitted derivative of Stokes I shown as smooth dotted curves. The value of B_θ fit for each position and its calculated error are given at the top of each plot.

Reynoso & Mangum (1999, in prep.) have detected CO(1-0) emission toward CTB37A with $\sim 1'$ resolution using the Kitt Peak 12m telescope. Their maps show two distinct CO clouds, one at ~ -22 km s $^{-1}$ in the northern part of CTB37A, and another at ~ -65 km s $^{-1}$ which is concentrated to the northwest and middle of the source. Both CO clouds are coincident spatially and in velocity with our two groups of OH (1720 MHz) masers.

3.2.4. CTB33

The SNR in CTB33 is also known as G337.0–0.1, and was estimated to lie at a distance of ~ 11

Fig. 7.— Continued...

kpc by Sarma et al. (1997) using HI absorption data from the ATCA (Australia Telescope Compact Array). These authors also find that CTB33 has a spectral index of ~ -0.6 , typical of shell type SNRs. The locations of the two bright OH (1720 MHz) masers from Frail et al. (1996) are shown on Figure 8 superposed on a 1380 MHz CTB33 continuum image (Sarma et al. 1997). However, Sarma et al. (1997) present evidence that the southern most CTB33 maser is probably associated with the HII region G336.9–0.2. Our OH (1720 MHz) results are consistent with this suggestion since this maser feature has been resolved into at least four different velocity components, each of which show complicated Stokes V spectra typical of HII region masers (i.e. no “S” shaped Zeeman pattern; see Elitzur 1998). For this reason only the centrally located CTB33 maser (CTB33 OH(1)) has been included in Tables 2 and 3. The B_θ detected for this maser is 1.1 mG, but the range of channels over which the fit was performed had to be limited to obtain a reasonable fit (see Fig. 9). Therefore, this detection should be considered tentative. Such a suppression of part of the Stokes V signal may be the result of blending of the maser line in velocity space since this maser is fairly wide ($\Delta v_{FWHM} \sim 1$ km s $^{-1}$, also see Roberts et al. 1993), but could also simply be a result of poor S/N.

Corbel et al. (1999) have detected a number of molecular clouds toward CTB33 in CO($J = 1-0$) and CO($J = 2-1$) emission using the SEST tele-

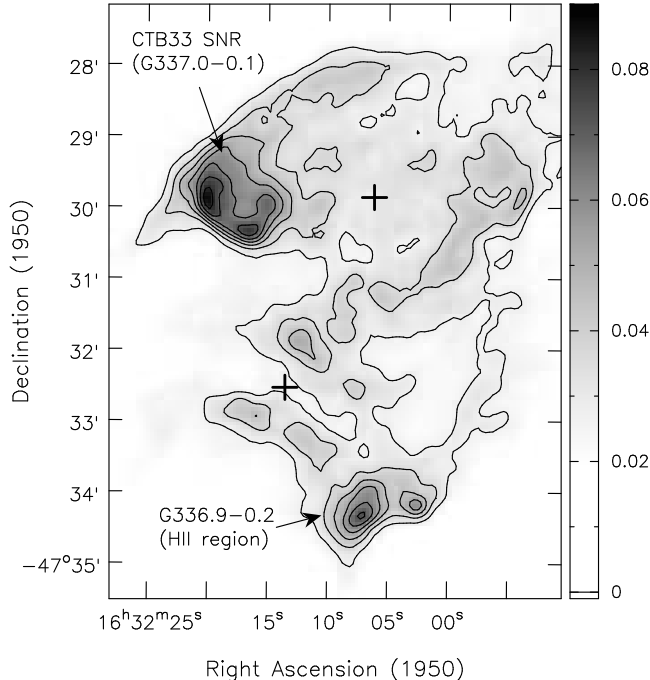


Fig. 8.— CTB33 1375 MHz ATCA continuum image from Sarma et al. (1997) with contours at (0.3, 0.4, 0.5, 0.6, 0.7, 0.8, 0.9) $\times 0.090$ Jy beam $^{-1}$. The resolution of this image is $\sim 12''$. The locations of the two CTB33 OH (1720 MHz) masers with $S_\nu > 200$ mJy are indicated by the black (+) symbols.

scope. In particular, they find a giant molecular cloud at a velocity of ~ -71 km s $^{-1}$ ($\Delta v = 11$ km s $^{-1}$) with an approximate size of 67 pc and a mass of $4 \times 10^6 M_\odot$. The velocity of this molecular cloud is in excellent agreement with the velocity of CTB33 OH(1) (-71.8 km s $^{-1}$) and may well be the origin of the SNR/molecular cloud interaction needed to pump the maser (see §1 & §4.2). These authors also suggest that the SNR must lie on the near-side of the ~ -71 km s $^{-1}$ GMC based on comparison of their CO data (and its implied extinction) with the X-ray data from Woods et al. (1999).

The CTB33 SNR is coincident with the site of a recently discovered Soft Gamma ray Repeater (SGR1627–41; see Hurley et al. 1999). The location of the SGR has been constrained by the 3rd Interplanetary Network (IPN: *Ulysses*, KONUS-WIND and BATSE) along with the detection of a presumably related BeppoSAX X-ray source to lie within the error boxes shown in Figure 10 on

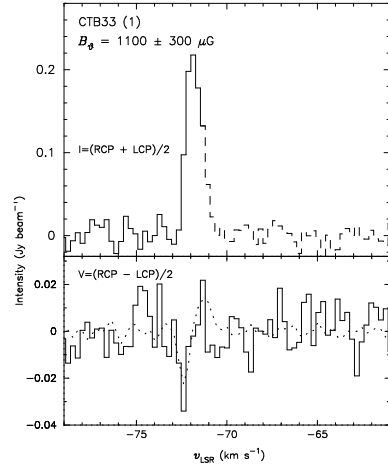


Fig. 9.— Fit of B_θ for CTB33 OH (1720 MHz) maser feature (1). The upper panels show the VLA Stokes I profiles (*solid histogram*), and the bottom panels show the VLA Stokes V profiles (*solid histogram*) with the fitted derivative of Stokes I shown as smooth dotted curves. The value of B_θ fit for each position and its calculated error are given at the top of each plot. The solid portion of the Stokes I histogram (*upper panel*) shows the velocity range used in the fit.

a simplified contour image of CTB33 (Sarma et al. 1997; Hurley et al. 1999; Woods et al. 1999). Current theories for the nature of SGRs suggest that they arise from strongly magnetized neutron stars or ‘magnetars’, and that the outbursts are the result of crustquakes on the surface of the neutron star (Thompson & Duncan 1995). The discovery of SGR1627–41, marks only the fourth such source to be detected.

All of the previously known SGRs have been associated with young SNRs (although SGR1900+14 lies close to, but not inside its associated SNR; see Hurley et al. 1999 and references therein). For this reason, despite the inexact correspondence between the IPN/BeppoSAX error boxes and the extent of CTB33 ($95''$) proposed by Sarma et al. (1997), SGR1627–41 has been assumed to be the progenitor of CTB33. For this reason, a number of authors (Hurley et al. 1999; Corbel et al. 1999) have estimated that SGR1627–41 must have a transverse velocity of more than $\sim 1,000$ km s $^{-1}$ if CTB33’s age is $\lesssim 5,000$ years. Although these velocities are not

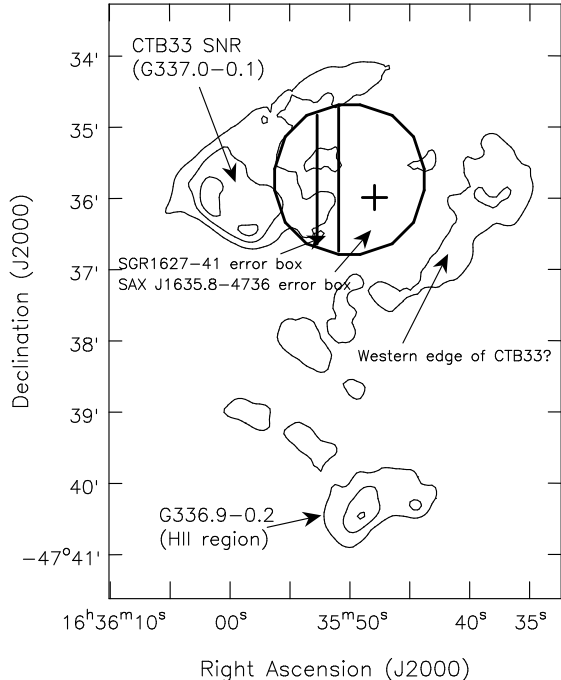


Fig. 10.— Similar to Figure 8, but in J2000 coordinates with contours at $(0.4, 0.6, 0.8) \times 0.090 \text{ Jy beam}^{-1}$. The IPN and BeppoSAX error boxes are superposed showing the location of SGR1627–41.

unreasonable (Lyne & Lorimer 1994), the location of the maser CTB33 OH(1) suggests that CTB33 actually extends farther west as shown in Figure 10, and has a ‘blowout’ morphology toward the NE and SW. Such a morphology would not be unexpected in a region populated by H II regions that could have effectively cleared such cavities (see Jones et al. 1998). Therefore, an increase in the estimated size of CTB33 would place the IPN/BeppoSAX error boxes and the OH (1720 MHz) maser much closer to the center of CTB33, rather than at its outskirts, with a substantial reduction in the estimate for the transverse velocity of SGR1627–41. Future molecular, or high resolution, low-frequency continuum data toward CTB33 may help resolve this issue.

3.2.5. G357.7–0.1 (*Tornado*)

G357.7–0.1 is an unusual SNR candidate located near the galactic center with a non-thermal spectral index in the range $-0.5 < \alpha < -1.0$

(Stewart et al. 1994). It has been variously considered to be everything from an extragalactic head-tail or double lobed source (Weiler & Panagia 1980; Caswell et al. 1989) to a new class of galactic head-tail object (Becker & Helfand 1985; Helfand & Becker 1985; see also Gray 1994). Another intriguing suggestion is that G357.7–0.1 is powered by an object ejected from the nearby SNR (G359.0–0.9) which lies only $1'$ from the symmetry axis of G357.7–0.1. This scenario, however, would require such a ‘runaway’ pulsar or X-ray binary to have a transverse velocity $\gtrsim 2,000 \text{ km s}^{-1}$ which is considered unlikely (Gray 1994). The discovery of a OH (1720 MHz) maser coincident with G357.7–0.1 has renewed speculation that it is, in fact, a galactic SNR (Frail et al. 1996).

The odd morphology of G357.7–0.1 has earned it the name ‘Tornado’. The reason for this moniker can be seen in the greyscale continuum images of G357.7–0.1 shown in Figure 11 (see also, Shaver et al. 1985a; Becker & Helfand 1985). Figure 11a was created from archival VLA data at $\sim 6 \text{ cm}$ from both C and D configuration data. The resulting image has a resolution of $13.4'' \times 6.7''$ (P.A. = 23.8°) and an rms of $\sim 0.6 \text{ mJy beam}^{-1}$. The data used to create the image in Figure 11b were compiled from 18 cm and 20 cm VLA archive data from all four VLA configurations. The resulting image is one of the most sensitive and highest resolution images of this source to date with an rms of $\sim 1.5 \text{ mJy beam}^{-1}$ and resolution of $11''.6 \times 8''.1$ (P.A. = 26.2° ; see also Shaver et al. 1985a; Becker & Helfand 1985; Yusef-Zadeh 1999b). Comparison of the peak flux densities in Figs. 11a ($S_{6\text{cm}} = 77 \text{ mJy beam}^{-1}$) and 11b ($S_{20\text{cm}} = 145 \text{ mJy beam}^{-1}$) confirms that the spectral index of G357.7–0.1 is ≈ -0.5 .

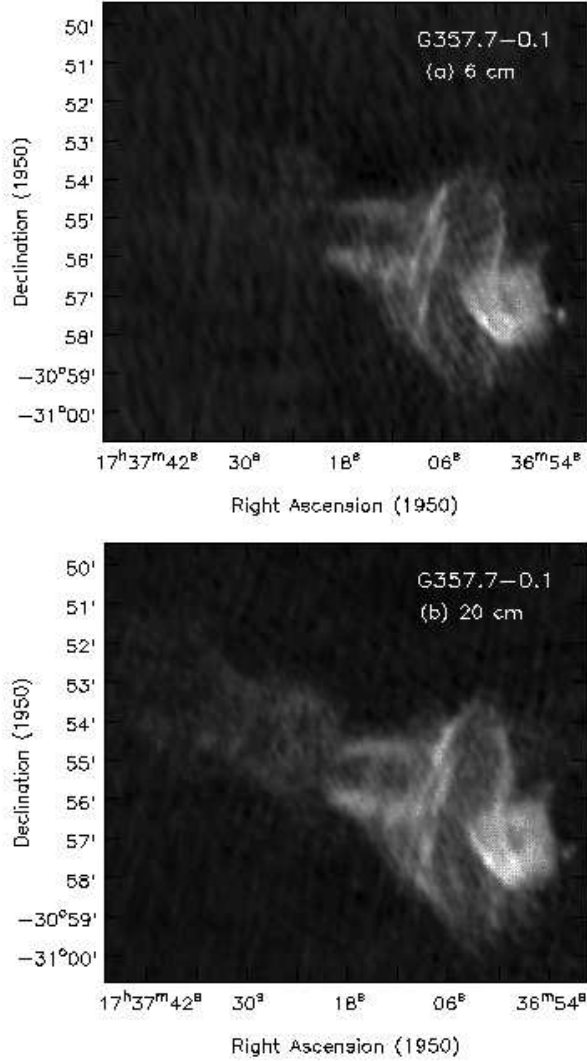


Fig. 11.— Greyscale continuum images of G357.7-0.1 composed of archival VLA data showing its spiral morphology. a) 6 cm image with a resolution of $13''.4 \times 6''.7$ (P.A. = 23.8°) and a peak flux density of 77 mJy beam^{-1} with an rms noise of $\sim 0.6 \text{ mJy beam}^{-1}$. b) Same as a) but at 20 cm. The resolution of the 20 cm image is $11''.6 \times 8''.1$ (P.A. = 26.2°) and the peak flux is $145 \text{ mJy beam}^{-1}$ with an rms noise of $\sim 1.5 \text{ mJy beam}^{-1}$.

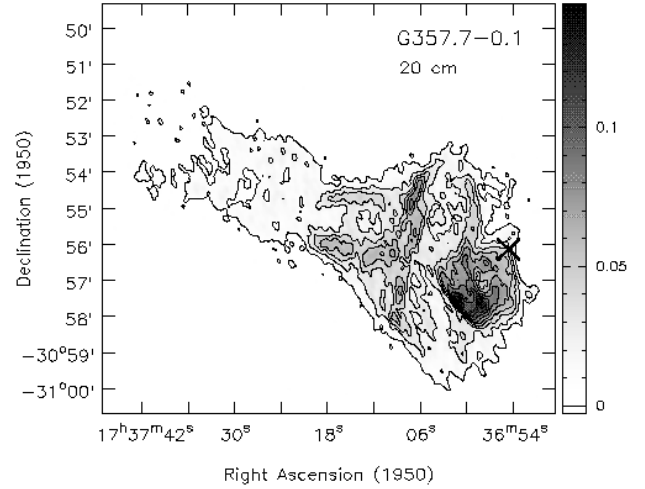


Fig. 12.— Similar to Figure 11b, but with contours at $(0.05, 0.15, 0.25, 0.35, 0.45, 0.55, 0.65, 0.75, 0.85) \times 145 \text{ mJy beam}^{-1}$. The location of G357.7-0.1 OH (1720 MHz) maser feature (1) is marked by an (x) symbol.

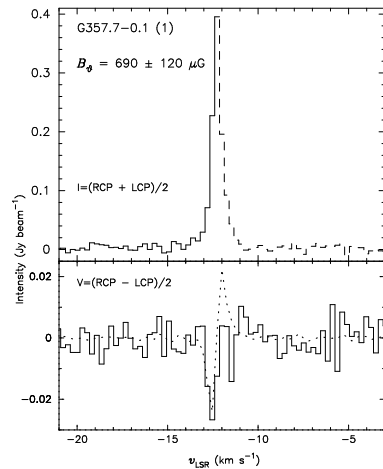


Fig. 13.— Fit of B_θ for G357.7-0.1 OH (1720 MHz) maser feature (1). The upper panels show the VLA Stokes I profiles (solid histogram), and the bottom panels show the VLA Stokes V profiles (solid histogram) with the fitted derivative of Stokes I shown as smooth dotted curves. The value of B_θ fit for each position and its calculated error are given at the top of each plot. The solid portion of the Stokes I histogram (upper panel) shows the velocity range used in the fit.

A compact source at the western edge of G357.7–0.1 is also apparent in Figs. 11a and b (also observed by Shaver et al. (1985b); see also Stewart et al. 1994, and references therein). We obtain flux densities of 70 ± 4 mJy and 69 ± 12 mJy for this compact source at 6 cm and 20 cm respectively, confirming that this source has a flat spectrum as suggested by Shaver et al. 1985b. At the resolution of the 18 cm A-array data ($4''.5 \times 3''.4$) this source is extended and has a diameter of $\sim 6''$ with a possible extension to the east (toward the SNR). The exact nature of this source remains unknown. Shaver et al. (1985b) cite its flat spectral index at radio wavelengths as evidence that it is an unrelated H II region. Alternatively, Shull, Fesen, & Saken (1989) suggest that it could be a pulsar which is interacting with the SNR shell and is responsible for the peculiar morphology of G357.7–0.1 similar to CTB 80. Higher resolution continuum observations or recombination line observations of this compact source are needed to determine its nature.

Figure 12 shows the 20 cm image (similar to Fig. 11b) with the single G357.7–0.1 OH (1720 MHz) maser superposed. The fit of this maser’s $B_\theta = 0.7$ mG is shown in Figure 13. For this maser feature, only the high velocity side of the line could be adequately fit by the derivative of Stokes I. As mentioned for CTB33 OH(1), a suppression of part of the Stokes V signal can be due to the presence of more than one velocity component, but the narrowness of this line ($\Delta v_{FWHM} \sim 0.6$ km s $^{-1}$) makes either an inability to fully resolve the Stokes V pattern or poor S/N more probable explanations. In the absence of better data, this detection should be regarded as tentative. Yusef-Zadeh et al. (1999b) also observed G357.7–0.1 at 1720 MHz with the VLA in A-configuration during an OH (1720 MHz) survey of the Galactic center. With their short integration time (rms ~ 12 mJy), they were able to place an upper limit on B_θ for G357.7–0.1 OH(1) of 2 mG, consistent with our 0.7 mG detection. In addition, these authors detected extended OH (1720 MHz) emission toward G357.7–0.1 with the VLA in D-

configuration ($114'' \times 38''$ resolution). These authors note that this extended emission may originate from low-gain masers given the lack of OH (1720 MHz) absorption toward this source.

Linear polarization images of the synchrotron emission from G357.7–0.1 at 5.8 GHz by Stewart et al. (1994) show that the plane-of-sky magnetic field vectors lie circumferentially to the vertical bands of continuum emission (best seen in Fig. 11). These authors note that this morphology is suggestive of a spiral magnetic field structure in the SNR. It is also interesting to note that the Stewart et al. images indicate a lack of linear polarization at the location of the OH (1720 MHz) maser, as might be expected if \vec{B} were nearly along the line of sight.

4. DISCUSSION

4.1. Implications from 1720 MHz Maser Theory

We have assumed until now that magnetic fields can be calculated from the Zeeman effect in masers using the same formalism that has been developed for thermal radiation (i.e. Troland & Heiles 1982 and B_θ in Table 3). However, stimulated emission is intrinsically different from spontaneous emission or absorption (see Elitzur 1996), so it is not unreasonable to imagine that a maser’s polarization properties are different from those of thermal emission. A common variable in any polarization study is the ratio of the line splitting ($\Delta \nu_B = Z | \vec{B} |$) to the Doppler width ($\Delta \nu_D$) which we will denote x_B . In what follows we assume this ratio is small ($x_B \ll 1$) since we do not resolve the line splitting in our Stokes I spectra (i.e. the splitting is only detected in Stokes V). In this section we review the results of several theoretical maser polarization studies for the case $x_B \ll 1$ (Elitzur 1996, 1998; and Nedoluha & Watson 1992) and compare the implications and predictions of these studies to the currently available OH (1720 MHz) Zeeman data. These comparisons have not proven sufficient to discern exactly how the total maser magnetic field strength $| \vec{B} |$ scales with our thermal estimates B_θ (Table 3), but have led to a number

of related conclusions which are described below.

One recent analytical study of the polarization properties of masers by Elitzur (1998) has suggested that the usual thermal Zeeman formulation, $V = ZC|\vec{B}|dI/d\nu$ with C a constant, may not be valid for unsaturated masers. Unfortunately, a key uncertainty in the study of masers is that their degree of saturation cannot be observed directly. However, Elitzur (1998) also proposes that a maser’s saturation state can be revealed by the ratio of its Stokes V profile to the derivative of Stokes I (i.e. $\mathcal{R}=V/(dI/d\nu)$). This is a consequence of the fact that maser amplification during unsaturated maser growth is exponential, causing a narrowing of the maser line. Under these circumstances, Elitzur (1998) predicts that $\mathcal{R}= ZC|\vec{B}|$ is not a constant (i.e. $C \neq \text{constant}$) and instead assumes a Gaussian absorption shape.

A test of this prediction was performed for the \mathcal{R} profiles of W51C feature 2 (dynamic range = 720:1) and the highest dynamic range maser in the Claussen et al. (1999) VLBA study of W28 (W28 F39 [A]; dynamic range = 60:1). Note, that the VLBA OH maser data have three times the spectral resolution of the VLA data. The \mathcal{R} profiles for both of these masers are relatively flat (to within their rms) and show no evidence of the Gaussian absorption shape predicted for unsaturated maser emission. We conclude however, that while these \mathcal{R} profiles are indicative of saturated maser emission, this test is somewhat impractical for real data. The derivative of I passes through zero at line center by definition, and toward the line wings as well depending on the rms of the spectra. A more useful variation of this test is to investigate the linear dependence of Stokes V as a function of $dI/d\nu$ since this test does not suffer from the discontinuities that are inevitable with the \mathcal{R} test. The resulting V vs. $dI/d\nu$ plots reveal the straight lines expected from saturated emission (i.e. $ZC|\vec{B}| = \text{constant}$) for W51C OH(2) and W28 F39 [A] along with several more of the masers in this study (i.e. G349.7+0.2 OH(3), CTB37A OH(1-5)), but remain inconclusive for the lowest S/N masers (i.e. CTB33 OH(1)).

Another perspective on a maser’s degree of saturation can be gained by comparing an upper limit for its optical depth (τ_{max}) assuming that it *is* unsaturated, with a lower limit (τ_{min}) based on the flatness of its observed \mathcal{R} ratio. For unsaturated masers, $T_b = T_x \exp(\tau_{max})$ (where τ_{max} is the maser’s optical depth at line center and T_x is the excitation temperature; see Elitzur 1998 for details). As mentioned above, the lower limit depends on the confidence with which a flat \mathcal{R} profile can be determined, so that $\tau_{min} = \epsilon^{-1} \ln \mathcal{D}$, where ϵ is the dynamic range of the observations and \mathcal{D} is $\sigma_{B_\theta}/B_\theta$ (Elitzur 1998). Elitzur (1998) notes that whenever these two limits are inconsistent ($\tau_{min} > \tau_{max}$), the maser must be saturated. This ‘inconsistency’ was found to be true for every maser in our sample, indicating that OH (1720 MHz) masers may indeed be saturated. This was also found to be the case in a OH (1720 MHz) maser study of the galactic center by Yusef-Zadeh et al. (1999a). We point out, however, that we have only been able to calculate a lower limit for T_b since the maser spots are not resolved at the present resolutions. This means that if the true values of T_b (and hence τ_{max}) are large enough, the apparent saturated maser inconsistencies ($\tau_{min} > \tau_{max}$) could disappear. However, the sizes found for OH (1720 MHz) masers in the W28 and W44 VLBA observations of Claussen et al. (1999) $\sim 50 - 180$ mas, if typical, imply that the majority of masers in this study would still have $\tau_{min} > \tau_{max}$ as required for saturated maser emission.

Even if these masers are likely to be saturated, a second intrinsic uncertainty in performing Zeeman analysis on OH masers is the value that should be taken for the constant “ C ” in $V = ZC|\vec{B}|I'$. According to Elitzur (1998), this constant is modified from its thermal value: $C_{th} = \cos \theta$ to $C_m = 8/(3p \cos \theta)$ for saturated masers, where θ is the angle between the magnetic field vector and the line-of-sight. This solution to the maser polarization problem takes into account the fact that a photon generated via stimulated emission does not necessarily have the same polarization as the parent photon, and that the radiation is beamed. The parameter p in

this formulation depends on the geometry of the masing region, with $p = 1$ or 2 for filamentary or planar geometry respectively. Notice that in addition to the factor of $8/(3p)$ difference between the thermal and maser equations for $|\vec{B}|$, they also have a completely different dependence on $\cos\theta$. That is, while thermal radiation samples $B_{los} = |\vec{B}| \cos\theta$, masers sample $B_m \propto |\vec{B}| / \cos\theta$ according to the Elitzur model. Therefore, this model suggests that the magnetic field needed to produce a maser's Stokes V signal is *less* than the field needed to produce a comparable signal from thermal radiation (i.e. $C_m > C_{th}$). For example, using $|\vec{B}| = (B_\theta/C_m)$, the Elitzur (1998) model predicts $|\vec{B}| = 0.3pB_\theta$ for $\theta = 35^\circ$, and $|\vec{B}| = 0.1pB_\theta$ for $\theta = 75^\circ$.

Ideally, the Stokes parameters U, Q, and V should only depend on θ and $|\vec{B}|$. Therefore, if analytic expressions for the Stokes parameters are known, it should be possible to calculate θ and $|\vec{B}|$ explicitly. According to Elitzur (1996), the analytic expression for the linear polarization fraction ($|q| = (Q^2 + U^2)^{1/2}/I$) has the approximate form

$$q \approx \left[1 - \left(\frac{2}{3 \sin^2 \theta} \right) \right], \quad (1)$$

as long as $x_B \ll 1$. Therefore, if the linear polarization fraction is known, Eq. [1] can provide an estimate for θ and hence the magnitude of C_m . For the case of W51C OH(2), where we have measured $q = 3.5\%$ (§3.2.1), we obtain $\theta \approx 56^\circ$ and $C_m \approx 5/p$. Consequently, in the Elitzur model, W51C OH(2) has $|\vec{B}| \approx (0.4 \times p)$ mG compared to its estimated thermal B_θ value of 1.9 mG (where $p = 1$ or 2).

Unfortunately, this technique can only produce accurate results if the “total” linear polarized intensity is measured. The more extensive Stokes Q and U observations of OH (1720 MHz) masers in W28 and W44 (Claussen et al. 1997), indicate that q only ranges from 0.5% to 22% for all 30 of the masers with positive Q and U detections. In fact, the linear polarization of the masers in W28 and W44 is quite low with average values of $4 \pm 5\%$ and $10 \pm 5\%$ respectively, similar to that found for W51C OH(2) (\pm gives the standard deviation of the distribution). It

would be quite remarkable if q , and hence the angle between the line-of-sight and the magnetic field (θ), were so similar in three different SNRs. Indeed it would be more natural for the polarized intensity of these masers to be more widely varied as is the case for SiO masers (see for example McIntosh & Predmore 1993). There are at least two other effects in addition to the viewing angle (θ) which can decrease the magnitude of q . These are 1) Faraday depolarization within the masing region and 2) curvature of the magnetic field lines within the masing region causing cancellation within the beam (i.e. MHD waves, see Elitzur 1992).

Faraday rotation can only be a significant factor if the Faraday rotation sizescale is smaller than the length scale of the masing region (see Elitzur 1992 for details). From Elitzur (1992) the Faraday rotation sizescale is $\ell_F = 2 \times 10^{16} (\lambda^2 n_e B_{los})^{-1}$ where λ is the observing frequency in cm, n_e is the electron density in cm^{-3} , and B_{los} is the magnitude of the magnetic field along the line of sight in Gauss. Theoretical modeling of OH (1720 MHz) masers by Lockett et al. (1999) and Wardle (1999) suggest that the ionization fraction needed to produced a large enough column of OH for strong maser action is in the range $10^{-7} \lesssim \chi_e \lesssim 10^{-5}$. These authors also find that the density in the masing region must lie in the range $1 \times 10^4 \text{ cm}^{-3} \lesssim n_{H_2} \lesssim 5 \times 10^5 \text{ cm}^{-3}$. Given our average magnetic field detection of $B_\theta \sim 1$ mG, the Faraday rotation length scale can be written

$$\ell_F = 6.2 \times 10^{17} \left[\left(\frac{n_{H_2}}{10^5 \text{ cm}^{-3}} \right) \left(\frac{\chi_e}{10^{-6}} \right) \left(\frac{B_{los}}{1 \text{ mG}} \right) \right]^{-1} \text{ cm}. \quad (2)$$

This ℓ_F estimate is only three times larger than the OH (1720 MHz) maser gain length estimated by Lockett et al. (1999) of $\sim 2 \times 10^{17}$ cm, implying that Faraday depolarization may contribute to the low linear polarization intensities observed by Claussen et al (1997). The decrease of polarization intensity with increasing J in SiO masers is also thought to be a consequence of such Faraday depolarization (McIntosh & Predmore 1993; or Wallin & Watson 1997 for an opposing view). Unfortunately, the magnitude of such depolarization is difficult to quantify and quite model dependent (see e.g. Wallin & Watson 1997).

In addition, some evidence of tangling in the magnetic field lines may be indicated from the ten-fold increase in B_θ measured toward W28 F39 [A] with the VLBA (~ 2 mG) compared to the average value measured throughout W28 with the VLA (~ 0.2 mG; Claussen et al. 1999). However, this particular spot did not have a positive VLA B_θ detection (due to the presence of multiple spatial components at the lower resolution) so a direct comparison is not possible. More VLA vs. VLBA magnetic field strength comparisons are needed to determine whether this apparent increase in B_θ with higher resolution is real and/or common.

These examples suggest that the linear polarization intensities observed toward W51C, W28, and W44 could be reduced from their ‘true’ values by one or both of these effects, making the calculation of θ directly from q unreliable. Alternatively, using the condition that $q^2 + v^2 \leq 1$, (where $v = V/I$), it is possible to obtain the following constraint on θ at the frequency of the peak in Stokes V, $16(x_B)^2 \lesssim \cos^2 \theta \lesssim 2/3$ as long as $x_B < 0.2$ (see Elitzur 1996 for details). This means that the angle between \vec{B} and the line of sight must be greater than $\sim 35^\circ$ in order for polarized emission to be observed at all (see also Goldreich, Keeley, & Kwan 1973). This lower limit on θ ($\sim 35^\circ$), suggests that the magnetic field values reported in Table 3 (B_θ) are *overestimated* by factors of at least 1.5 ($p = 2$). The upper bound on θ cannot be accurately calculated from these data since it depends on x_B ($ZB_\theta/\Delta\nu_D$) and our current spectral resolution (0.27 km s^{-1} ; the highest available with the VLA in 2IF mode) is insufficient to resolve line splittings with $x_B < 0.2$. However, since B_θ is an *upper limit* on the total field strength ($|\vec{B}|$), a useful limit on x_B can be made by taking the average value of $B_\theta/\Delta\nu_{FWHM}$ using data from Tables 2 and 3, in which case $x_B \lesssim 0.12$ on the average and $\theta \lesssim 61^\circ$. This upper limit to θ suggests that the average total field strength is $|\vec{B}| \gtrsim 0.2pB_\theta$, i.e. the thermal approximation (B_θ in Table 3) *overestimates* the maser field ($|\vec{B}|$) by less than a factor of $C_m \sim 5/p$.

It is important to note, however, that the

analytic expressions formulated by Elitzur are controversial and that other maser studies have reached different conclusions. For example, the numerical simulations of Nedoluha & Watson (1992) suggest that if $x_B \ll 1$ and the maser is not *strongly* saturated, the thermal Zeeman relationship is a good approximation (i.e. $C_m \sim 1$). Unfortunately, it is quite difficult to compare the two methods since the Elitzur model is an analytical treatment, while the Nedoluha & Watson (1992) result arises from a numerical simulation. Also notable is the Nedoluha & Watson (1990) finding that it is very difficult to produce linear polarization in masers unless they are at least *partially saturated*. It is impossible to make any quantitative statements on this issue with the data presented here since we only attempted linear polarization measurements toward one of our sources (W51C). However, the Claussen et al. (1997) OH (1720 MHz) maser study of all four Stokes parameters toward the SNRs W28, W44, and IC443 contains a total of 49 masers with $S_\nu > 200$ mJy. About 60% of these have positive Q and/or U detections. In addition, all 13 of the Claussen et al. (1997) masers with 3σ B_θ detections also have positive Stokes Q and/or U detections. These comparisons suggest that in the Nedoluha & Watson model strong OH (1720 MHz) masers are also likely to be at least partially saturated.

An additional observational test offered by maser theory is to check whether there is any correlation between the linear polarization position angle (P.A.) and the SNR shock front in the vicinity of a maser spot. Several studies have suggested that OH (1720 MHz) masers must arise in shocks which are propagating transverse to the line of sight (Lockett et al. 1999; Wardle 1999; Frail & Mitchell 1998; Claussen et al. 1997). It is also likely that the magnetic field vector lies preferentially in the plane parallel to the shock front since only this component can be amplified by shock compression. In addition, the linear polarization P.A. for masers, unlike that of thermal dust emission, can be either parallel or perpendicular to the direction of the magnetic field in the plane of the sky. This difference occurs be-

cause the asymmetry of dust grains removes one degree of freedom. For these reasons, we might expect the observed P.A. of the linear polarization to be either parallel or perpendicular to the shock front. Of course such a comparison is only meaningful if significant Faraday rotation of the P.A. has not occurred either because the Faraday depolarization is insignificant or because the P.A. of the linear polarization is unaffected by it. A lack of *net* P.A. rotation in the presence of depolarization is suggested by Elitzur (1992) and the SiO maser observations of McIntosh & Predmore (1993), although Wallin & Watson (1997) present an alternate viewpoint based on numerical simulations.

For the case of W44 region E, the linear polarization angle is $\sim -28^\circ$ (Claussen et al. 1997) and the OH (1720 MHz) masers are also distributed along a line which is oriented NW/SE at about the same angle. Further indication of the orientation of the shock front comes from CO ($J = 3 - 2$) observations by Frail & Mitchell (1998) which show a ridge of shocked CO emission parallel to the line of masers. This example suggests that there is a correlation between OH (1720 MHz) linear polarization position angles and the orientation of the shock front. The presence of such a correlation could argue against the possibility of significant Faraday rotation within the SNRs or may result from Faraday depolarization without significant net rotation. In any case, additional linear polarization measurements in conjunction with molecular observations of OH (1720 MHz) maser regions are needed to confirm this connection.

These comparisons between observation and theory of OH (1720 MHz) masers have led to the following conclusions: (1) It is likely that OH (1720 MHz) masers are saturated based on their flat \mathcal{R} profiles (determined directly and from estimates of maser optical depths; Elitzur 1998). This conclusion is also supported by the high incidence of linear polarization in these masers (Nedoluha & Watson 1992; Claussen et al. 1997). (2) The linear polarization intensities of OH (1720 MHz) masers (needed to calculate $|\vec{B}|$ in the Elitzur model) may be significantly reduced

from their intrinsic values by Faraday rotation and/or by tangling in the magnetic field lines. This also means that it is impossible to calculate the reduction of $|\vec{B}|$ compared to B_θ using these data directly ($|\vec{B}| \propto B_\theta \cos \theta$). However, for angles between 35° and 75° , the Elitzur model predicts that the total magnetic field strength should range from $|\vec{B}| = (0.3 - 0.1)pB_\theta$ (where $p = 1$ or 2 for filamentary or planar geometry respectively). Alternatively the numerical simulations of Nedoluha & Watson (1992) suggest that this correction factor is essentially unity. (3) It may be possible to predict the direction of the shock in which an OH (1720 MHz) maser arises from the position angle of its observed linear polarization (as long as the P.A. is not significantly rotated by Faraday rotation).

4.2. Magnetic Fields in Shocked Molecular Gas

In this study we have reported ten new measurements of OH (1720 MHz) Zeeman magnetic field strengths in five galactic SNRs. Previous studies of this type (Claussen et al. 1997; Koralesky et al. 1998; Yusef-Zadeh et al. 1996) have measured B_θ in an additional five SNRs. The magnitude of B_θ in all of these SNRs (including those measured here) have typical values between 0.1 and 4 mG. However, as the discussion in §4.1 demonstrates, the conversion factor between thermal estimates of B_θ and the true maser field $|\vec{B}|$ is uncertain. Therefore, although we will continue to reference our measured fields B_θ (Table 3), it should be kept in mind that B_θ could be an upper limit that overestimates the true field by less than a factor of five.

Maser theory suggests that OH (1720 MHz) masers originate in shocked molecular clouds (e.g. Lockett et al. 1999; Wardle 1999). If so, the measurements reported here of B_θ (and in the references cited above) must originate in post-shock gas. These theories suggest that OH (1720 MHz) masers can only be pumped efficiently for densities in the range $1 \times 10^4 \text{ cm}^{-3} \lesssim n_{H_2} \lesssim 5 \times 10^5 \text{ cm}^{-3}$ and temperatures in the range $50 \text{ K} \lesssim T \lesssim 125 \text{ K}$ (see Lockett et al.

1999). Indeed, when independent measurements of the conditions in the post-shock gas have been made (see Frail & Mitchell; Reach & Rho 1998, 1999) the gas properties are in agreement with these theoretical expectations.

It remains an open question how magnetic fields of these strengths are generated; i.e. shock compression vs. turbulent amplification (Jun & Norman 1996). In what follows we will show that compression of the existing ambient molecular cloud field is all that is required to produce the observed field strengths. One further argument against significant turbulent amplification of the fields is the likelihood of destroying the maser action due to loss of velocity coherence in a turbulent velocity field.

A number of Zeeman studies have been undertaken in the past decade to detect magnetic fields in molecular clouds for the purpose of studying star formation (e.g. Roberts et al. 1993; Brogan et al. 1999). In a recent review by Crutcher (1999) of the existing data for star forming regions, the magnetic field was found to scale with density as $|\vec{B}| \propto n^{0.47}$. Crutcher notes that there are two possible physical interpretations for this relationship: (1) Such a relationship between $|\vec{B}|$ and n has been predicted by Fiedler & Mouschovias (1993) based on studies of ambipolar diffusion; (2) A similar relation is suggested by the observed invariance of the Alfvénic Mach number $m_A = \sqrt{3}\sigma/V_A \approx 1$ in molecular clouds, where $V_A = |\vec{B}| / 4\pi\rho^{1/2}$ and $\sigma = \Delta v / (8 \ln 2)^{1/2}$ (see Bertoldi & McKee 1992; Zweibel & McKee 1995). This invariance implies $|\vec{B}| \propto \Delta v \sqrt{\rho}$.

For the range of gas densities expected in OH (1720 MHz) maser regions ($1 \times 10^4 \text{ cm}^{-3} \lesssim n_{H_2} \lesssim 5 \times 10^5 \text{ cm}^{-3}$; Lockett et al. 1999), the range of magnetic fields predicted by the relation $|\vec{B}| \propto n^{0.47}$ is $75 \mu\text{G}$ to $475 \mu\text{G}$. Clearly the OH (1720 MHz) B_θ measurements reported in this work (Table 3) are greater than those predicted by Crutcher’s relation (see also Figure 14). However, there is a great deal of uncertainty in this statement since Crutcher considers B_{los} ($B_{los} = |\vec{B}| \cos \theta$) which *underestimates* the field by factors of ~ 2 while our determination of B_θ could *overestimate* the field by as much as a fac-

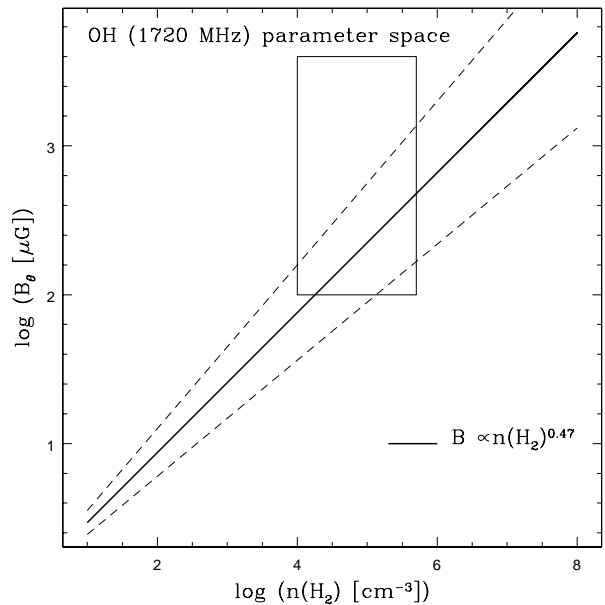


Fig. 14.— Plot of $B_\theta \propto n^{0.47}$ (Crutcher 1999; solid thick line) with the OH (1720 MHz) maser’s B_θ parameter space superposed. The two dashed lines show the 1σ errors on the fit obtained by Crutcher.

tor of five according to the Elitzur model (see §4.1).

If we assume, however, that the two types of magnetic field measurements (molecular cloud vs. OH (1720 MHz) masers) are approximately comparable (i.e. the thermal Zeeman equation is valid for masers) it may not be surprising that their magnitudes are different. This is because theory and observations suggest that OH (1720 MHz) masers do not originate in undisturbed “normal” molecular clouds, but rather have experienced a shock (see above). If this is the case, the Bertoldi & McKee interpretation for the scaling of $|\vec{B}|$ ($\propto \Delta v \sqrt{\rho}$) suggests that OH (1720 MHz) masing regions simply have larger linewidths for a given density than unshocked molecular clouds. If we set $V_A = \sqrt{3}\sigma$ as suggested by Bertoldi and McKee (1992), then $|\vec{B}| = 0.4\Delta v n_p^{1/2}$ where n_p is the proton density in cm^{-3} and the line width (Δv) is in km s^{-1} . For the case of the W51C OH (1720 MHz) masers, we can take $\Delta v = 10 \text{ km s}^{-1}$ based on the CO observations of Koo (1999), and $n_p = 1 \times 10^5$

cm^{-3} from the typical density needed to excite OH (1720 MHz) masers (Lockett et al. 1999; Wardle et al. 1999). With these estimates, the implied magnetic field strength is $|\vec{B}| = 1.3 \text{ mG}$, in close agreement with the B_θ values observed toward W51C.

Alternatively, if the B_θ 's measured in OH (1720 MHz) masers should be reduced by factors of $\lesssim 5$ (i.e. Elitzur's maser polarization model), the fields estimated from OH (1720 MHz) masers are in agreement with the values predicted by Crutcher's relation. In this case, the magnetic fields in masing regions and molecular clouds follow the same scaling with density without shock amplification of the field, i.e. no Δv dependence. Such agreement might be expected if the observed scaling were the result of ambipolar diffusion in both types of regions. Clearly convergence on our understanding of the nature of maser polarization (and hence $|\vec{B}|$) is needed to distinguish between the two possibilities.

In a radiative shock, compression of the gas follows the relation $\eta = \sqrt{2}V_s/V_{Ao}$, where V_{Ao} is the Alfvén velocity in the pre-shock gas (see Draine & McKee 1993). Using the relation $B_o \propto n_o^{1/2}$, it can be shown that $V_{Ao} \simeq 2 \text{ km s}^{-1}$ (see also Heiles et al. 1993). Thus for reasonable shock velocities (10 - 50 km s^{-1} ; Lockett et al. 1999; Frail & Mitchell 1998), $\eta = 7 - 35$. This compression is sufficient to enhance B_o to B_θ without invoking turbulent enhancement of the magnetic field, assuming that $B_{ps}/B_o = \eta$ (see Chevalier 1999; Frail & Mitchell 1998). For example, if we take a typical shock speed of $V_s \sim 25 \text{ km s}^{-1}$ and typical values of $B_o \sim 70 \mu\text{G}$ for molecular clouds of density $n_o \sim 5 \times 10^3 \text{ cm}^{-3}$ (Frail & Mitchell 1998; Wardle 1999; Crutcher 1999), $\eta \approx 18$ and $B_{ps} \sim 1.2 \text{ mG}$ - in close agreement with the observed values of B_θ . This demonstration shows that typical cloud and shock parameters can lead to enhancement of the pre-shock magnetic fields to the observed values of B_θ .

4.3. Energetics Implied by Observed B_θ

Using the thermal Zeeman equation, we have detected magnetic fields (B_θ) between 0.2 and 2 mG (Table 3) in OH (1720 MHz) masers associated with five galactic SNRs. However, as described in §4.1 these thermal field strengths may *overestimate* the "true" field strength $|\vec{B}|$ by a factor between $\sim 2 - 5$ (i.e Elitzur 1998). Alternatively, other theoretical studies suggest that B_θ is a good approximation to $|\vec{B}|$ (i.e. Nedoluha & Watson 1992). For this reason, along with our inability to calculate the exact correction factor in the Elitzur model, we have chosen to use B_θ in the calculations below. However, the fact that B_θ could be an upper limit to the magnetic field strength should be kept in mind.

Regardless of the exact details of the B_θ to $|\vec{B}|$ conversion or the origin of these fields (argued to be shock compression of the ambient field above), it is clear that the OH (1720 MHz) fields are strong (compared to those found in dark clouds $\sim 30 \mu\text{G}$, for example). This is an important finding since the magnetic field plays a key role in many aspects of the SNR/molecular cloud interaction including : (1) As noted above, the magnetic field determines and, in fact, limits the amount of shock compression in the post-shock gas. (2) Magnetic support may help stabilize the post-shock cloud, via the magnetic force acting on ions perpendicular to the magnetic field lines. (3) In the model of Lockett et al. (1999), heating by ambipolar diffusion is needed to extend the length of time the post-shock gas spends at temperatures favorable to OH (1720 MHz) maser inversion. Ambipolar diffusion is also thought to be the method by which subcritical clouds dissipate their magnetic energy and form stars (Ciolek & Mouschovias 1995). Given the many roles that the magnetic field can play in the evolution of a shocked cloud, we estimate the magnetic energy compared to other energy sources within the region below.

From the values of B_θ listed in Table 3 the magnetic pressure ($P_{B_{ps}} = B_{ps}^2/8\pi$), in the post-shock gas of the five SNRs studied here, ranges

from 10^{-7} to 10^{-9} erg cm $^{-3}$. These values are large compared to both P_{ISM} ($\sim 5 \times 10^{-13}$ erg cm $^{-3}$) and $P_{thermal}$ of the hot X-ray emitting gas interior to the remnant, $\sim 2 \times 10^{-10}$ erg cm $^{-3}$ (Kulkarni & Heiles 1988; Frail & Mitchell 1998; Claussen et al. 1997). From the X-ray observations of Koo et al. (1995) of W51C ($n_e = 0.3$ cm $^{-3}$; $T_e = 3 \times 10^6$ K), we can estimate directly that $P_{thermal} = 2n_e k T_e \approx 3 \times 10^{-10}$ erg cm $^{-3}$ for this SNR. The ram pressure of the shock can also be compared to $P_{B_{ps}}$ since they should be approximately equal if the field strengths are proportional to the amount of shock compression, i.e. $B_{ps}^2/8\pi = \rho_o V_s^2$. For example, using the values of n_o and V_s estimated in §4.2 ($n_o = 5 \times 10^3$ cm $^{-3}$ and $V_s = 25$ km s $^{-1}$), $\rho_o V_s^2 = 5 \times 10^{-8}$ erg cm $^{-3}$. The equivalent magnetic pressure for W51C OH(1) ($B_\theta = 1.5$ mG) is 9×10^{-8} erg cm $^{-3}$, in close agreement with the estimated ram pressure. Therefore, the magnetic pressure in the post-shock gas dominates over the thermal pressure of the SNR but is approximately equal to its ram pressure. The fact that the ram pressure is almost three orders of magnitude larger than the thermal pressure of the shock indicates that this SNR is in the radiative phase as expected for SNRs with OH (1720 MHz) masers.

5. SUMMARY AND CONCLUSIONS

We have observed the OH (1720 MHz) line in five galactic SNRs to measure their magnetic field strengths using the Zeeman effect. We detected all 12 of the bright ($S_\nu > 200$ mJy) OH (1720 MHz) masers previously observed by Frail et al. (1996) and Green et al. (1997) and measured significant magnetic fields (i.e. $> 3\sigma$) in ten of them. The estimated field strengths, which we denote B_θ , range from 0.2 to 2 mG and are in good agreement with those measured in the five other SNR (0.1 - 4 mG) for which Zeeman OH (1720 MHz) maser studies exist (Koralesky et al. 1997 and references therein). In these studies, the field strengths were calculated using the thermal Zeeman equation for Zeeman splitting less \ll the line width (i.e. $V = Z B_\theta dI/d\nu$). In this formula, the total field strength ($|\vec{B}|$) is related to B_θ by $|\vec{B}| = B_\theta/C_m$ where C_m is a function

of the viewing angle θ ($C_m = \cos \theta$ for thermal emission). However, there exists some controversy about the θ dependence of C_m for saturated masers and whether it is even a constant for unsaturated masers (see §4.1). For example, in the Elitzur (1998) model $C_m \propto 1/(\cos \theta)$ for masers. *From comparison of these data with maser polarization studies we conclude that these OH (1720 MHz) masers are likely to be saturated and that $C_m \lesssim 5$, i.e. the B_θ values reported in Table 3, overestimate the actual field strengths ($|\vec{B}|$) by less than a factor of five.*

We estimate that these magnetic field strengths are consistent with the hypothesis that ambient molecular cloud B-fields are compressed via the SNR shock to the observed values (§4.2). Indeed, field strengths of this magnitude exert a considerable influence on the properties of the shocked cloud. For example the magnetic pressures estimated from the values of B_θ listed in Table 3 ($10^{-7} - 10^{-9}$ erg cm $^{-3}$) far exceed the pressure in the ISM or even the thermal pressure of the hot gas interior to the remnant (§4.3). We also find that this range of magnetic pressures is in very good agreement with the ram pressure expected from C-type radiative shocks.

In §4.2 and §4.3 we show that there is excellent agreement between our values of B_θ and those implied by shock compression and ram pressure using typical values from the literature. It is somewhat difficult to maintain this agreement if B_θ should be reduced by as much as a factor of $\lesssim 5$ (i.e. Elitzur's maser polarization model §4.1), although there is probably sufficient uncertainty in the parameters to allow such fine-tuning. We also show that the observed values of B_θ for OH (1720 MHz) masers are greater than those observed in molecular clouds for the same range of densities (Crutcher 1999). It is possible that this difference is due the intrinsic physical nature of the $|\vec{B}| \propto n^{1/2}$ relation (§4.2) or may be the result of overestimating the maser B-fields (§4.1).

In the future, knowledge of the field strength could be used in conjunction with molecular data to study the physics of these molecular shocks in more detail. In one such study Frail & Mitchell

(1998) mapped the distribution of molecular gas in the vicinity of several masers spots in W28 and W44 with the JCMT. These observations revealed that the OH masers are preferentially located along the edges of thin filaments or clumps of molecular gas, suggesting compression of the gas by the passing shock. In addition to this morphological evidence, the density, temperature and velocity dispersion of the gas at these locations suggested that the OH (1720 MHz) masers originate in post-shock gas. Combining the VLA and JCMT data they were able to show directly that the magnetic pressure dominates over the thermal pressure in the post-shock gas, balancing against the ram pressure of the gas entering the shock wave (i.e. $B_{ps}^2/8\pi = \rho_o V_s^2$). Thus OH (1720 MHz) measurements of B_θ lead to constraints on the physics of these molecular shocks that are difficult to obtain any other way. When used in conjunction with molecular observations, it should be possible to fully specify the properties (i.e. geometry, density, temperature, velocity) of C-type shocks.

C. Brogan would like to thank NASA/EPSCoR for fellowship support through the Kentucky Space Grant Consortium, as well as, summer student support from NRAO. We would also like to thank M. Elitzur and G. Nedoluha for useful discussions on maser theory and M. Claussen for providing his VLBA W28 data and useful comments on the manuscript. In addition, we thank the anonymous referee for many useful suggestions.

REFERENCES

- Becker, R. H., & Helfand, D. J. 1985, *Nature*, 313, 115
- Bertoldi, F., & McKee, C. F. 1992, *ApJ*, 395, 140
- Brogan, C. L., Troland, T. H., Roberts, D. A., & Crutcher, R. M. 1999, *ApJ*, 515, 304
- Caswell, J. L., Kesteven, M. J., Bedding, T. R., & Turtle, A. J. 1989 *Proc. Astron. Soc. Aust.*, 8, 184
- Chevalier, R. A. 1999, *ApJ*, 511, 798
- Ciolek, G. E. & Mouschovias, T. Ch. 1995, *ApJ*, 454, 194
- Claussen, M. J., Frail, D. A., Goss, W. M., & Gaume, R. A. 1997, *ApJ*, 489, 143
- Claussen, M. J., Frail, D. A., Goss, W. M., & Desai, K. 1999, *ApJ*, 522, 349
- Corbel, S., Chapuis, C., Dame, T. M., & Durouchoux, P. 1999, *ApJ*, in press
- Crutcher, R. M. 1999, *ApJ*, 520, 706
- Dickel, J. R., van Breugel, W. J. M., & Strom, R. G. 1991, *AJ*, 101, 2151
- Draine, B. T., & McKee, C. F. 1993, *ARA&A*, 31, 373
- Elitzur, M., 1992 *Astronomical Masers* (Dordrecht:Kluwer), 6.8
- Elitzur, M. 1996, *ApJ*, 457, 415
- Elitzur, M. 1998, *ApJ*, 504, 390
- Fiedler, R. A., & Mouschovias, T. Ch. 1993, *ApJ*, 415, 680
- Frail, D. A., Goss, W. M., & Slysh, V. I. 1994, *ApJ*, 424, L111
- Frail, D. A., Goss, W. M., Reynoso, E. M., Giacani, E. B., Green, A. J., & Otrupcek, R. 1996, *AJ*, 111, 1651
- Frail, D. A., & Mitchell, G. F. 1998, *ApJ*, 508, 690
- Goldreich, P., Keeley, D. A., & Kwan, J. Y. 1973, *ApJ*, 179, 111
- Gray, A. D. 1994, *MNRAS*, 270, 835
- Green, A. J., Frail, D. A., Goss, W. M., & Otrupcek, R. 1997, *AJ*, 114, 2058
- Heiles, C., Goodman, A. A., McKee, C. F., & Zweibel, E. G. 1993, *Protostars and Planets III*, ed. E.H. Levy & J. I. Lunine (Tucson: Univ. of Arizona Press), 279167-181
- Helfand, d. J. & Becker, R. H. 1985, *Nature*, 313, 118
- Hurley, K., Kouveliotou, C., Woods, P., Mazets, E., Golenetskii, S., Frederiks, D. D., Cline, T., & Van Paradijs, J. 1999, *ApJ*, 519, L143
- Jones, T. w., Rudnick, L., Jun, B., Borkowski, K. J., Dubner, G., Frail, D. A., Kang, H., Kassim, N. E., & McCray, R. 1998, *PASP*, 110, 125
- Jun, B. & Norman, M. L. 1996, *ApJ*, 472, 245
- Kassim, N. E., Baum, S. A., & Weiler, K. W. 1991, *ApJ*, 374, 212
- Klein, R. I., McKee, C. F. & Colella, P. 1994, *ApJ*, 420, 213

- Koo, B. -C., Kim, K. -T., & Seward, F. D. 1995, *ApJ*, 447, 211
- Koo, B. -C., & Moon, D. -S., 1997a, *ApJ*, 475, 194
- Koo, B. -C., & Moon, D. -S., 1997b, *ApJ*, 485, 263
- Koo, B. -C. 1999, *ApJ*, 518, 760
- Koralesky, B., Frail, D. A., Goss, W. M., Claussen, M. J., & Green, A. J. 1998, *AJ*, 116, 1323
- Kulkarni, S. R., & Heiles, C. 1988, *Galactic & Extragalactic Radio Astronomy* (2nd edition) Berlin and New York, Springer-Verlag, 95
- Lockett, P., Gauthier, E., & Elitzur, M. 1999, *ApJ*, 511, 235
- Lyne, A. G., & Lorimer, D. R. 1994, *Nature*, 369, 127
- McIntosh, G. C., & Predmore, C. R. 1993, *ApJ*, 404, L71
- MacLow, M.-M., McKee, C. F., Klein, R. I., Stone, J. M., & Norman, M. L., 1994, *ApJ*, 433, 757
- Miesch, M. S. & Zweibel, E. G. 1994, *ApJ*, 432, 622
- Milne, D. K. 1990, in *Proc. 140th IAU Symp., Galactic and Intergalactic Magnetic Fields*, Beck, B., Kronberg, P. P., & Wielebinski, R., ed., 67
- Nedoluha, G. E., & Watson, W. D. 1990, *ApJ*, 354, 660
- Nedoluha, G. E., & Watson, W. D. 1992, *ApJ*, 384, 185
- Reach, W. T., & Rho, J. 1998, *ApJ*, 507, L93
- Reach, W. T., & Rho, J. 1999, *ApJ*, 511, 836
- Roberts, D. A., Crutcher, R. M., Troland, T. H., & Goss, W. M. 1993, *ApJ*, 412, 675
- Sarma, A. P., Goss, W. M., Green, A. J., & Frail, D. A. 1997, 483, 335
- Shaver, P. A., Salter, C. J., Patnaik, A. R., van Gorkom, J. H. & Hunt, G. C. 1985a, *Nature*, 313, 113
- Shaver, P. A., Pottasch, S. R., Patnaik, A. R., van Gorkom, J. H. & Hunt, G. C. 1985b, *A&A*, 147, L23
- Shull, M. J., Fesen, R. A., & Saken, J. M. 1989, *ApJ*, 346, 860
- Stewart, R. T., Haynes, R. F., Gray, A. D., & Reich, W. 1994, *ApJ*, 432, L39
- Subrahmanyan, R., & Goss, W. M. 1995, *MNRAS*, 275, 755
- Thompson, C., & Duncan, R. C. 1995, *MNRAS*, 275, 255
- Troland, T. H., & Heiles, C. 1982, *ApJ*, 260, L19
- Wallin, B. K., & Watson, W. D. 1997, *ApJ*, 481, 832
- Wardle, M., Yusef-Zadeh, F. & Geballe, T. R. 1999, in *ASP Conf. Series, Vol. 186. The Central Parsecs*, Falcke, H., Cotera, A., Duschl, W. J., Melia, F. & Rieke, M. J., ed., 432
- Wardle, M., 1999, *ApJ*, 527, L109
- Weiler, K. W., & Panagia, N. 1980, *A&A*, 90, 269
- Woods, P., Kouveliotou, C., Van Paradijs, J. Hurley, K., Kippen, R. M., Finger, M. H., Briggs, M. S., Dieters, S., & Fishman, G. J. 1999, *ApJ*, 519, L139
- Yusef-Zadeh, F., Roberts, D. A., Goss, W. M., Frail, D. A., & Green, A. J. 1996, *ApJ*, 466, L25
- Yusef-Zadeh, F., Roberts, D. A., Goss, W. M., Frail, D. A., & Green, A. J. 1999a, *ApJ*, 512, 230
- Yusef-Zadeh, F., Goss, W. M., Roberts, D. A., Robinson, B. & Frail, D. A. 1999b, *ApJ*, in press
- Zweibel, E. G., & McKee, C. F. 1995, *ApJ*, 439, 779

This 2-column preprint was prepared with the AAS L^AT_EX macros v4.0.